

Physically Plausible Adaptive Variable Density Sampling Scheme based on Artificial Bee Colony (ABC) using Modified Projection Constraints

Akshay Kumar Jagadish^a, Kasi Rajopal^b

^a*Electrical and Electronics Engineering, NITK, Surathkal.*

^b*Electrical Engineering, Indian Institute Of Science, Bangalore.*

Abstract

There are many swarm optimization algorithms that are motivated by the hierarchical working, efficient self-organizing skills and highly developed foraging ability of the bee population in nature. In this paper, we propose a novel data-driven algorithm, using swarm intelligence of artificial bee colony (ABC), called k -ABC, to generate an adaptive variable density sampling (VDS) scheme for compressive sampling (CS) based data acquisition for fast MR imaging. The algorithm exploits the behaviour of the three types of bees - scout-bees, employed-bees and onlooker bees, with certain modifications based on the characteristics of variable density sampling. We introduce the concept of searching for the high quality food sources in annular regions of varying widths, called as bins, to optimise the process of foraging. The k -ABC algorithm uses magnitude k -space distribution of a reference single-slice MR image as the underlying fitness value distribution to generate an adaptive sampling scheme. We have also addressed the problem of designing a tailor-made template sampling scheme for 3D volume MR imaging for the very first time. Retrospective CS-MRI simulations show that the proposed k -ABC adaptive VDS scheme shows significant improvement over other sampling schemes for both single slice and multi-slice MR imaging. Further, for the task of implementation, a modified projection algorithm, that takes into account the physical constraints of gradient and slew-rate, has been introduced which provides a significant improvement in the reconstructed image quality with minimum trade-off in terms of scan-time.

Keywords: Artificial Bee Colony (ABC), k -ABC, Compressive sampling (CS), Variable Density Sampling (VDS).

1. Introduction

Magnetic Resonance Imaging (MRI) is a versatile tool used in diagnostic, functional, structural and molecular level studies. In medical imaging, MRI is a non-invasive and radiation safe imaging modality used for diagnosing a range of life threatening diseases as it offers a variety of contrast mechanisms and enables excellent visualization of both anatomical structure and physiological function. The major drawback of MRI is the significantly long scan time taken for data acquisition which affects imaging throughput and image quality, especially in dynamic imaging applications. The reason for the slow data acquisition is that only few samples of k -space can be acquired in a single RF (Radio Frequency) excitation and readout. The RF excitation has to be repeated sequentially several times to obtain the k -space samples required for the full FOV (Field of View) reconstruction. Therefore, many techniques have been developed for increasing the scanning speed by faster data collection made possible by designing geometrical trajectories, efficient and fast pulse sequences, and hardware techniques. These faster scanning methods have reached a saturation, defined by physical limits of hardware and the physiological limits of the human body. Compressed Sensing (CS) [?], a sparse signal recovery technique, is being widely used to reconstruct MR (magnetic resonance) images since it requires only few non-uniform measurements, unlike traditional Nyquist uniform sampling, provided the underlying image has sparse representation in some transform domain (like Fourier domain), and the acquired samples are incoherent in the same domain. Thus, CS provides an alternate framework, for fast data acquisition in MRI, by acquiring only few k -space samples with significant energy for reconstruction.

Several variable density sampling (VDS) methods have been proposed to reduce the scan time by significantly sub-sampling the k -space randomly and use CS techniques to reconstruct MR images with good quality and resolution.

These VDS methods have a deterministic fully sampled dense central region and random sampling of rest of the k -space based on an underlying probability distribution function (pdf) approximating the magnitude spectrum of a target k -space distribution. The VDS methods in literature can be classified based on pdf defined by 1) mathematical distribution functions or 2) magnitude spectrum of reference template image (known as adaptive sampling). The methods based on reference template image are known as adaptive sampling however both types of methods adapt to the underlying specified pdf.

Lustig et al. [?] developed the idea of randomized Cartesian sub-sampling for application of compressed sensing to rapid and high quality MR imaging. The random sampling concept was extended to draw samples from a polynomial based probability density function (pdf) using Monte-Carlo algorithm such that it has lowest mutual coherence with the sparsifying transform. However, constructing a pdf that will generate a suitable sampling pattern with appropriate number of low and high frequency k -space samples is a challenging problem.

Wang et al [?] have proposed a pseudo 2D random sampling using two 1D VDS that are orthogonal to each other in Cartesian k -space, also with a dense central region. In [?], Boyer et al. have generalized CS results from independent drawing of isolated measurements to independent drawings of blocks of measurements. In this work, blocks could be chosen arbitrarily which represent continuous trajectories. More importantly, these authors have provided closed form expressions for the optimal distribution on the block set. However, due to the restriction on the admissible blocks the possibility of its usage on a MR machine is low.

The adaptive sampling methods, which is the main focus, use the magnitude spectrum of a representative reference image as the pdf instead of mathematical distribution approximating the k -space distribution. The resulting sampling patterns in both cases adapt to the underlying specified pdf. Knoll et al. [?] have proposed adaptive random sampling scheme by using power spectrum of a reference image as templates for deriving a pdf. The property that various structures of the body share similar distribution of k -space magnitude and not

necessarily anatomical details is the basis for his approach.

Adcock et al. [?] have proposed an optimal multi-level random sub-sampling strategy based on the structure of the signal which is shown to give better results than the uniform random sub-sampling. The authors also address the design of sampling schemes by accounting for a simple structured sparsity hypothesis; assuming that wavelet coefficients become sparser as the resolution increases. In essence, implying that the low frequencies of a signal should be sampled deterministically.

An adaptive sampling algorithm using a novel sparsifying Dictionary Learning technique which simultaneously learns an image patch based dictionary and reconstructs the image using under-sampled data iteratively has been proposed by Ravishankar et al. [?] which shows significant improvement over other VDS schemes.

Travelling Salesman Problem (TSP) based optimization for sampling pattern generation has been proposed by Chauffert et al. [?]. In this method, a continuous k -space trajectory is traced using sample points drawn from a specific target distribution (π -distribution) by solving TSP.

Jaganathan et al. [?] have proposed the concept segmenting the phase encode direction and random sampling in each phase encode segment to improve the distribution of undersampling locations for better reconstruction performance.

Chennakeshava et al. [?] have designed two adaptive variable density sampling scheme based on a novel approach of binning the pdf derived from the fully sampled k -space spectral energy distribution of a reference image. In the first method, the normalized k -space histogram is binned exponentially, and the resulting pdf information matrix is used with a suitable control parameter to obtain a sampling pattern of desired undersampling ratio. In the second method, the binning of the k -space distribution is followed by ranking of the bins by its spectral energy content. The samples are selected from the energy rank ordered bins using a Knapsack constraint such that the normalized energy preservation factor (NEPF) is maximized and the sampling points selected from

the highly relevant bins giving a very robust sampling pattern with well defined sparsity level.

Designing a sampling pattern with optimal number of low and high frequency k -space samples from an underlying pdf is a combinatorial optimization problem. Artificial bee colony (ABC) algorithm, a swarm intelligence algorithm motivated by the foraging behavior of bee swarms, is one such meta-heuristic bio-inspired optimization algorithm which has captured significant attention in many diverse fields including of biological simulation, traveling salesman problem, stochastic vehicle routing problem and also other neural network based algorithms. Karaboga et al. [?] developed an idea based on honey bee swarm for numerical optimization and then proposed a combinatorial ABC algorithm for solving traveling salesman problem. Later, an adaptive artificial bee colony algorithm was used by Rekaby et al [?] to solve the TSP but the fitness value solution of the food sources had no considerable improvement. Both traveling salesman and the vehicle routing problem both optimize the shortest available path with single or multi-slice constraints.

In the bee colonies in nature, the nectar collected by the bees are stored in cells of the hive. In MR imaging, sampling points that are closer to center of k -space similarly hold the essential features pertaining to overall structure of the image, contrast details and signal to noise ratio. Hence, certain region in the center of k -space, possessing high energy [?], is sampled densely which is analogous to the bee-hive. Further, this deterministic-like sampling with a set of highly coherent vectors also helps overcome the so-called "coherence barrier" in MR Imaging. The random sampling with variable sparsity from the center in k -space is similar to variation in the quantity and quality of food sources gradually with distance from the hive. The similarities, in central dense bee-hive and varying quantity and quality of food sources gradually with distance to k -space distribution in MR imaging, is the motivation for ABC based algorithm for sampling pattern generation.

In this paper, we have designed a meta-heuristic iterative artificial bee colony algorithm to mimic a VDS scheme for fast MR imaging. The standard ABC al-

gorithm is modified to introduce a novel concept searching in radial annular bins with varying cost function. It is shown that the proposed novel k -ABC based adaptive VDS sampling algorithm gives significant improvement over other well-known VDS algorithms.

2. **k -ABC Algorithm**

2.1. *Introduction to Bee Colony*

The model of forage selection that leads to the ascent of collective intelligence of bee swarms consists of *three* essential components [?]: food sources, employed bees and unemployed bees, and delineates two leading modes of the behavior: Recruitment to a nectar source and abandonment of a source.

(a) *Food Sources:*

The merits of a food source depend on myriad factors, such as its proximity to the nest, richness or concentration of energy and the ease of extracting this energy. The distribution of food sources is a function of radial distance from the hive and can be decreasing, increasing or constant. The merit or fitness of the food sources is governed by a probability distribution function.

(b) *Employed bees:*

The employed bees are associated with a particular food source, which they are currently employed at exploiting. They carry with them information about this particular source, its distance and direction from the nest and the profitability of the source and share this information with a certain probability.

(c) *Unemployed bees:*

The unemployed bees are looking for a food source to exploit. There are two types of unemployed bees: scouts searching the environment surrounding the nest for new food sources and onlookers waiting in the nest and finding a food source through the information shared by employed bees.

2.2. Algorithm

In nature, the nectar collected by the bees are stored in cells of the hive. In MR imaging, sampling points that are closer to center of k -space similarly hold the essential features pertaining to overall structure of the image, contrast details thus, contributing to a better signal to noise ratio. Hence, certain region in the center of k -space, possessing high energy [?], is sampled densely which is analogous to the bee-hive. The concept of variation in the quantity and quality of food sources gradually with distance from the hive has been used to design the k -space sampling scheme. In order to preserve randomness in sampling scheme necessary for compressed sensing based reconstruction, random vectors or agents called scout-bees have been utilized for foraging for best nectars globally. Employed and onlooker-bees are made to forage locally in the neighborhood so as to further fine-tune the components possessing higher fitness values that are usually concentrated close to the center of k -space. Thus, a meta-heuristic algorithm has been developed, given the better performance of heuristics, as follows:

(a) Initialization of k -space

The hive of the bee system is the center or source of bee-movement. In this work, the bee-hive is initialized at the center of k -space representing the high energy low frequency peak of the k -space. The concept of annular region known as bins is introduced for search by spanning the entire k -space by number of circular annular bins, and information regarding the quality and distance of the selected food sources is passed on to the employed and onlooker-bees in the hive. The number of food sources N_k picked by scout-bees per bin was chosen to vary exponentially with distance and is given by $N_k = N_0 * \exp(-z * r_k)$ where the initial food source quantity N_0 is user-specified and z is a constant whose magnitude determines the rate of decay of N_k and sign determines if N_k is decreasing ($z > 0$), constant ($z = 0$) or increasing ($z < 0$). The scout-bees search for N_k nectars from k^{th} annular bin, whose width can remain either constant or increase based on its distance from the hive. The radius r_k of the

bin is given by:

$$r_k = \begin{cases} r_{k-1} + c_k * \Delta r, & \text{if } k > 0 \\ r_{IN}, & \text{if } k = 0 \end{cases} \quad (1)$$

where Δr gives the incremental width of the annular region and c_k determines the relative bin width of successive bins. The initial radius r_{IN} , and Δr are user-specified values.

(b) Random Search by the Scout-Bees

A predefined number of scout-bees perform random search for nectars scattered either randomly or according to a chosen distribution or a reference template to provide the unemployed-bees with a corresponding number of random locations in each bin to start their search for food sources in the neighborhood of the hive. The location of food sources in k^{th} bin is given by:

$$x_i^k = (\text{rand}(0, 1)(r_k - r_{k-1}) + r_{k-1}, \theta), \quad \forall k \in \{1, 2, \dots, N_k\}, \theta \in [0, 2\pi] \quad (2)$$

where θ is a randomly chosen angle. $x_i^0 = (\text{rand}(0, 1) * r_{IN}, \theta)$ gives the location of food sources within r_{IN} . The fitness value of the food source at the location x_i^k is given by $f(x_i^k)$ representing the probability of the food source being picked. Its value can be chosen from a standard pdf (Gaussian) or any user-defined distribution which closely approximates the k -space distribution of the slice being imaged or k -space distribution of a reference MR image in case of an adaptive scheme. The food source selection mechanism of k -ABC is performed using this pdf as underlying distribution. The flow chart in Fig. 1 shows the random search by scout-bees in bins in k -space.

(c) Local Search By the Employed-Bees

M optimum-valued food sources, x_m^k are chosen from the N_k locations provided by the scout-bees. A neighborhood search is performed by employed-bees in form of local concentric circles of varying radii r_l until atleast one better position is found. If the bee fail to update its position in one cycle, they restart the process by searching in circles of larger radii, $r_{l+1} = r_l + l * \Delta r_l$. One

cycle is said to be completed after nectars at J locations, y_j^l with radius r_l have been inspected. If a high quality nectar is found by the bee in its path, it will repeat the same cycle with the updated position as its new center. Thus, the employed-bees not only exploit the food source in its memory but also explore for other nectars available in its neighborhood. This process is carried out by all employed-bees simultaneously (or in parallel) using a greedy selection mechanism. The location of the nectars inspected by employed-bees, in the neighborhood of each of the M nectars, is given by:

$$y_j^l = (r_l, \theta + j\Delta\theta), \quad j \in \{1, 2, \dots, J\}, \quad l \in \{1, 2, 3, \dots\} \quad (3)$$

subject to the constraint $r_l \leq r_s$

where y_j^l indicates the locations along the circumference of circle with radius r_l , $\Delta\theta = (2\pi/J)$ and r_s is maximum radial spread for search.

Further, a greedy nectar selection mechanism was designed as follows:

$$x_{i+N_k}^k := y_j^l, \quad i \in \{1, 2, 3, \dots\} \quad (4)$$

subject to the constraint: $\nabla f(y_j^l) \geq \nabla f(y_{j-1}^l)$

The equation implies that the nectars are chosen based on the gradient of the fitness function at those locations. These newly chosen profitable nectars are added to the N_k food sources already present in the each bin, based on its location in k -space. Thus, the effective number of points in each of the bin after updating is $N_k^e \geq N_k$. This phase of local search by employed-bees is shown in Fig. 1.

Path and time constraints are imposed on the employed-bees by restricting them within distance r_s and controlling the number of nectars being searched and their relative distances through $\Delta\theta$ and Δr_l . The parameter J determines the number of food sources searched within radius r_l .

(d) Advance of the Onlookers-Bees

A designated number of the onlooker-bees move towards the E best food source locations chosen from the N_k^e nectars obtained in (4)

if they exceed a threshold, f_{th} defined as follows:

$$x_e^k := x_i^k, \text{ if } f(x_i^k) > f_{th} \quad \forall i \in \{1, 2, \dots, N_k^e\}, e \in \{1, 2, \dots, E\} \quad (5)$$

where E was fixed to be 50% of the employed-bee swarm size. Suppose S onlooker-bees move to each of these E positions by mutual agreement. Since, only one onlooker-bee can reach the best position x_e^k at a time, the remaining $S-1$ bees will strive to occupy that position, but can only be in close proximity of x_e^k at the locations $x_{e'}^k$ such that:

$$|x_e^k - x_{e'}^k| < \epsilon \text{ and } f(x_{e'}^k) \leq f(x_e^k).$$

Since, there is a high probability of finding a better or an equally good food source in the neighbourhood of a high fitness nectar. The advance of the onlooker-bees is said to be completed when $S-1$ bees satisfying the above constraints occupy their respective positions. The net count of the number of bees in each bin after the advance of the onlookers is N_k^o . This result of this search phase is shown in Fig. 1. The aforementioned steps involved in the search procedure, explained in stages (a)-(d), has been summarised as an algorithm called k -ABC.

3. Results & Discussion

We have conducted simulations to demonstrate the performance of the proposed k -ABC based adaptive and non-adaptive VDS schemes for retrospective CS-MRI. Two images obtained from fully sampled k -space of in-vivo MR scan of brain and T2-Weighted Sagittal Spinal image as shown Fig. 2, dimension 512×512 , were used as reference images in the simulations. The former was obtained from Saiprasad et. al [?] and latter was from the American Radiology Services [?]. The image quality was evaluated using PSNR (Peak Signal to Noise Ratio) - Higher the value better is the reconstruction, HFEN (High Frequency Normalised Error) [?] - Lower the value the better and SSIM (Structural Similarity Index Measure) [?] - closer to one the better, were used as metrics for structural fidelity. The k -space has been mapped from $[-k_{max},$

k_{max}] to [-1, 1] for convenience. The variable c_k in (1) was chosen to be unity for all k resulting in a total of 12 bins of uniform width excluding the initial bin.

3.1. Reconstruction Method

Dictionary Learning technique (DLMRI) by Saiprasad and Yoram Bessler [?] was used for reconstruction. This method takes into account the original image and learns a dictionary with a user-defined patch size and extent of overlapping. The algorithm has two steps. The update of dictionary is performed with the help of K-SVD [?] and sparse encoding by orthogonal matching pursuit [?]. The reconstructed images were obtained by setting the Number of dictionary learning iterations = 10, Number of K-SVD iteration = 10, Image patch size = 36 with Sparsity $T_0 = 5$ and Simulated Noise Level = 0.005.

3.2. Effect of varying food source distribution with distance

The number of food sources picked by scout-bees per bin N_k was chosen to vary exponentially with distance and is given by $N_k = N_0 * \exp(-z * r_k)$ where initial food source quantity N_0 is user-specified and z is a constant whose magnitude determines the rate of decay of N_k and sign determines if N_k is decreasing ($z > 0$), increasing ($z < 0$) or kept constant ($z = 0$). The Table I shows the image quality measures of the DLMRI reconstructed brain images for the three food source distributions at under-sampling factors $R = 5\%, 10\%, 15\%$ and 20% . The underlying fitness function is Gaussian in this case. It is seen that the image quality metrics are very close when N_k is distributed uniformly or exponentially decreasing with distance. However, the results are not encouraging for N_k exponentially increasing with distance which can be attributed to the trade-off involved in giving high priority to bins located further away from k -space center. Therefore, the motivation for the bees to search for high quality nectars (synonymous with high energy k -space center) in the vicinity of the hive is justified by the exponentially decreasing food source distribution with distance and is chosen for all further simulations and analysis.

3.3. Insight into Parameter Selection

The k -ABC VDS algorithm is designed with 5 parameters. Simulations were performed by varying one parameter at a time while keeping all other parameters fixed to show the sensitivity of the parameter to undersampling percentage and the consistency in reconstruction quality.

1. The initial food source quantity N_0 is varied as 1000:50:1400. It is observed from Fig. 4(a) that the undersampling percentage (R) varies from 9.97% to 10.55% (with mean and variance of $R_\mu = 10.1$, $R_{\sigma^2} = 0.052$). The corresponding variation in PSNR is from 40.94 dB to 41.10 dB ($\text{PSNR}_\mu = 41.01$, $\text{PSNR}_{\sigma^2} = 0.0029$), the SSIM is 0.942 to 0.944 ($\text{SSIM}_\mu = 0.944$, $\text{SSIM}_{\sigma^2} = 4.59e-05$) and HFEN is 0.752 to 0.740 ($\text{HFEN}_\mu = 0.75$, $\text{HFEN}_{\sigma^2} = 9.49e-05$ can be observed in Fig. 4(b), (c) and (d) respectively).
2. The initial radius r_{IN} , which represents the bee-hive, is varied from 5:5:40. The Fig. 4(a)-(d) show the variation of undersampling, PSNR, SSIM and HFEN respectively. It is seen that the undersampling percentage (R) shows a steady rise initially with increasing r_{IN} and then drops after reaching the peak. This indicates that there exists an optimum value for r_{IN} and therefore an optimal number of food sources $x_{r_{IN}}^0$ therein. The bin at the origin can be dense, necessary for a VDS scheme, only if the number samples selected in the bin is close or equal to the maximum number it can hold. The reconstructions show change in PSNR from 38.24 dB to 40.57 dB ($\text{PSNR}_\mu = 40.80$, $\text{PSNR}_{\sigma^2} = 0.056$), SSIM between 0.942 and 0.944 ($\text{SSIM}_\mu = 0.943$, $\text{SSIM}_{\sigma^2} = 4.58e-07$), HFEN lying between 0.725 and 0.86 ($\text{HFEN}_\mu = 0.801$, $\text{HFEN}_{\sigma^2} = 0.002$).
3. The bin-width, Δr , is varied from 5:5:30 pixels units and the respective change in reconstruction quality has been shown in Fig. 4(a)-(d) respectively. The undersampling percentage shows monotonic decrease which is justified because the number of bins decrease as Δr increases and correspondingly the cumulative number of sampling points also decrease. The quality of reconstruction follows accordingly with PSNR :

43.04 to 39.92 ($\text{PSNR}_\mu = 41.3255$, $\text{PSNR}_{\sigma^2} = 1.2298$), $\text{SSIM} : 0.969$ to 0.930 ($\text{SSIM}_\mu = 0.9479$, $\text{SSIM}_{\sigma^2} = 2.0150\text{e-}04$), $\text{HFEN} : 0.345$ to 1.014 ($\text{HFEN}_\mu = 0.6938$, $\text{HFEN}_{\sigma^2} = 0.0580$).

4. The number of employed-bees is varied from 30:10:100. The Fig. 4(a)-(d) show the variation of undersampling, PSNR, SSIM and HFEN respectively. The undersampling percentage (R) correspondingly varies from 8.7% to 13.3% almost linearly. This indicates that a linear increase in undersampling percentage can be obtained by a corresponding linear variation in the employed-bee number. It is seen that PSNR varies from 40.32 dB to 41.80 dB ($\text{PSNR}_\mu = 41.38$, $\text{PSNR}_{\sigma^2} = 0.36$), SSIM varies between 0.93 to 0.96 ($\text{SSIM}_\mu = 0.951$, $\text{SSIM}_{\sigma^2} = 8.53\text{e-}05$) and HFEN from 0.50 to 0.92 ($\text{HFEN}_\mu = 0.66$, $\text{HFEN}_{\sigma^2} = 0.020$).
5. The r_s , radius of neighbourhood search, is changed from $N/4$ to $N/1.5$ where N is the size of the image. The Fig. 4(a)-(d) show the variation of undersampling, PSNR, SSIM and HFEN respectively. The PSNR varies in the range 37.28 dB to 43.01 dB ($\text{PSNR}_\mu = 38.16$, $\text{PSNR}_{\sigma^2} = 10.14$), SSIM between 0.88 to 0.96 ($\text{SSIM}_\mu = 0.92$, $\text{SSIM}_{\sigma^2} = 8.62\text{e-}04$) and HFEN lying between 2.78 to 0.41 ($\text{HFEN}_\mu = 1.60$, $\text{HFEN}_{\sigma^2} = 0.81$).

3.4. Image quality for different under-sampling percentages

Based on the parameter sensitivity analysis in section 3.3, two parameters - r_{IN} and Δr have been held constant throughout the simulations for the algorithm, the remaining three parameters were then found by performing Monte-Carlo study such that the desired under-sampling percentages are obtained within a tolerance of 0.01%. The parameters r_{IN} and Δr were set to 0.078 and 0.039 respectively. The underlying fitness distribution was Gaussian with $\mu = 0$ and $\sigma^2 = 0.39$.

Monte-Carlo simulations were performed over the set of parameters with the fitness function specified by the magnitude of the k -space of the brain image,

which resulted in about 60 sampling patterns for different under-sampling percentages. The brain images were reconstructed with these sampling patterns for different under-sampling percentages and the image quality metrics were evaluated. The Table 2 shows the image quality metrics of the DLMRI reconstructed images for under-sampling percentages $R = 5\%, 10\%, 15\%$ and 20% . The best PSNR, HFEN and SSIM obtained from Monte-Carlo simulations are highlighted for the under-sampling percentage, while the mean and variance are shown in the next column. It is seen that the mean of the image quality metric match closely with the best result and the corresponding variances are small indicating the consistency of the reconstruction quality irrespective of the combination of the parameters that generate the sampling pattern. Three sampling schemes randomly chosen from Monte-Carlo samples for each undersampling percentage has been shown in Figure 4.

3.5. Robustness of the k -ABC Algorithm

The convergence of the k -ABC algorithm to a desired undersampling was tested, keeping the parameters fixed to those obtained via Monte-Carlo simulation (explained in section 3.4) and running it multiple, about 100, times . These parameters were chosen as reference since they had resulted in best image quality metrics for a given undersampling. The quality of reconstruction was evaluated for all the resulting converged sampling schemes. Though the resultant sampling patterns were not identical, the reconstruction quality metrics show high degree of consistency. The variance of the image quality metrics for undersampling of 10% and 5 % are $\text{PSNR}_{\sigma^2} = 0.0016$, $\text{SSIM}_{\sigma^2} = 3.1360\text{e-}07$, $\text{HFEN}_{\sigma^2} = 8.1047\text{e-}05$; and $\text{PSNR}_{\sigma^2} = 0.0268$, $\text{SSIM}_{\sigma^2} = 1.1913\text{e-}06$, $\text{HFEN}_{\sigma^2} = 0.0027$ respectively. It can be observed that the variance is small. Therefore, the algorithm converges well, resulting in good quality sampling patterns consistently.

It should be noted that the variance provided in Table 2 differs from the above, in that that the former shows that the reconstruction quality is consistent irrespective of combination of parameters that yield a given undersampling percentage,

while the latter shows that the algorithm converges to a efficacious sampling scheme given a fixed set of parameters.

3.6. *k*-ABC Adaptive VDS scheme performance

The ability of the proposed *k*-ABC sampling scheme to adapt to the underlying fitness distribution is shown in Fig. 6. The Gaussian distribution was considered since it captures the typical exponentially decaying distribution of the *k*-space in MRI images, while the π distribution [?] was chosen since it has been shown to be optimal in orthogonal system. And it minimizes the upper bound of Rauhut's [?] result (Theorem 4.2, 4.4) such that it meets the sparsity constraint of CS sampling. In the adaptive sampling scheme, normalized magnitude spectrum of *k*-space from fully sampled MR scan of the region of interest is the underlying fitness distribution for the algorithm.

Table 2, shows that the *k*-ABC adaptive sampling schemes for brain image give enhanced performance values for PSNR, HFEN and SSIM for different undersampling percentages of 20%, 15%, 10% and 5% respectively. Table 3 shows a comparison of reconstruction results of *k*-ABC sampling scheme (adaptive, non-adaptive and switched fitness-distribution i.e. using the distribution derived from sagittal image), and the non-adaptive VDS schemes for brain image with 10% and 5% undersampling where it is seen that the adaptive *k*-ABC performs significantly better. The image quality indices show similar trend in the case of T2-Weighted Sagittal Spinal image in the Table 4. The following observations are made

1. In general, it is observed that the *k*-ABC sampling scheme gives reconstruction performance within 0.5 dB irrespective of the underlying fitness function from which the sampling pattern is derived. It performs better than Saiprasad's adaptive scheme and Chauffert's independent π distribution scheme.
2. It can also be observed that the best performance is obtained for the adaptive sampling scheme with the fitness distribution from reference im-

age slice(s). The robustness of the k -ABC sampling scheme is evident (Table 3) as the image quality measures are close when the sampling pattern derived from a sagittal spine image k -space distribution is switched in reconstructing the brain image. The SSIM is almost identical for the two under-sampling percentages. A similar observation can be made from Table 4 for the sagittal spine image.

3. The reconstructed images using k -ABC adaptive sampling scheme with different underlying distributions for cases shown in Table 3 and 4 for brain and sagittal spine respectively for undersampling of 10% have been shown in Fig.7.

We show the reconstructed brain images in Fig. 13 for $R = 5\%$ and 10% . The images in left column show the k -ABC adaptive sampling pattern and Saiprasad adaptive pattern for $R = 5\%$ and 10% alternatively while the right column show their corresponding reconstruction of the brain image. The inset in the left corner shows the magnified image of the patch in the rectangle. It is seen that the k -ABC sampling scheme is able to reconstruct with good fidelity at low under-sampling percentage of 5%. The Fig. 4 shows comparison of the normalized line intensity profile of the original and reconstructed images along the vertical line (shown in Fig. 2 (Left)) to demonstrate its ability to capture the fine intensity structural variations in the reconstruction for even 5% under sampling.

3.7. Sampling Scheme for Multi-slice/ROI Volume Imaging

During image acquisition using MRI, multiple slices of region of interest (ROI) of the body are obtained referred to as ROI volume. To the best of our knowledge, none of the existing compressive sampling methods have addressed the problem of generating a data-driven adaptive sampling scheme, taking into account the whole volume. If a robust sampling pattern that can provide high reconstruction quality while scanning the entire ROI volume (either slice-by-slice or in 3D) is generated, it would considerably speed up the scan time.

We show that a template sampling scheme can be generated using the proposed k -ABC adaptive sampling scheme with normalized k -space computed from image of MR scan as underlying distribution. Given such an optimal sampling pattern, it can both be implemented as 3-D MR scanning by fixing the readout in orthogonal direction or using the slice-by-slice method but without generating sampling scheme for each slice. Volumes of two regions of interest, Knee and Brain, were investigated in search of an optimal slice by comparing the reconstruction performance of sampling schemes generated from different slices. However, finding an optimal sampling scheme is an optimization problem. We propose a simple method to generate a reference template fitness distribution for k -ABC algorithm that outperforms the sampling pattern generated using image slice(s) data.

3.7.1. Knee and Brain Volume Imaging:

T2-weighted FSE (Fast Spin Echo)images of knee acquired every 4mm; with TR = 4200 ms, TE = 99.1 ms and FS = 1.5; and having a total of 22 slices was considered [?]. The slices of the knee were divided into four groups based on 20 mm thickness in each group assuming that the anatomic differences between consecutive slices in not significant. First slice was chosen from each group and sampling scheme was generated using its normalized magnitude spectrum of k -space as underlying fitness distribution. Following which all 22 slices were reconstructed using the sampling scheme as reference. It can be observed in Fig. 10 that quality metrics (PSNR, HFEN and SSIM) match closely for all slices. The difference in quality, was not significant. To make use of the entire data, a mean normalized k -space was computed by averaging the normalized magnitude spectrum of k -space of all slices.

It was observed that the sampling scheme generated using it as underlying distribution, gives better performance for most of the imaging slice indices as seen in Fig. 10. Thus, the the mean normalized k -space distribution should be used as reference for generating sampling scheme.

In order to test the observations and inferences made with knee volune, 22

T1-weighted Spin echo MR image slices of brain acquired at every 5 mm; with TR = 450 ms and TE = 10 ms; were considered [?]. In this case, four slices of the brain volume were chosen randomly as reference and the the steps discussed earlier were retraced. It was observed that the reconstruction performance for all slices of the brain volume in terms of PSNR, HFEN and SSIM was similar as seen in Fig. 11. Further, the sampling scheme using the mean normalized k -space distribution the gives better performance in comparison to random reference slices that were chosen.

Thus, it is seen from the knee and brain volume imaging experiment that the sampling scheme can be generated, retrospectively, using mean normalized k -space distribution as reference, gives the best performance in terms of reconstructed image quality.is not much affected. It is extremely useful if only one slice or just a few slices of imaging data is available prior to the scan. However, if partial data is available either mean normalized template should computed or underlying k -space distribution derived from one of the slice should serve as reference. In conclusion, the proposed method will be extremely useful given the data of all slices of a specific ROI and will be preferred over sampling schemes, generated retrospectively, using each slice separately.

3.8. Practical Implementation

Designing an optimal physically plausible k -space trajectory, for fast and efficient scanning in MR imaging, has always been a challenging task [?]. Deriving motivation from Lustig et al. [?], Chauffert et al. [?] have proposed that it is better to project TSP solved trajectory of the sampling pattern onto a convex set of admissible curves instead of parametrization of the given trajectory. Chauffert designed a first order dual algorithm which provides theoretical guarantee in the form of rate of convergence satisfying smoothness of trajectory while minimizing the distance between the original sample and the projected sample location by iteratively projecting onto a convex set of admissible curves. The algorithm has properties of preserving the density of input curve, having the flexibility to smooth high curvature regions in the trajectory and impose

additional affine constraints including hardware-based gradient and slew rate. Chauffert et al. [?] projection and smoothing method is summarized before we propose a modified algorithm.

Designing the sampling trajectory, $s : [0, T] \rightarrow \mathbb{R}^d$, involves the following steps:

1. Find an input curve (admissible or otherwise) c with good distribution.

The TSP solution though sub-optimal, the only reasonable fast method since finding a shortest pathway amongst these samples of a VDS scheme is a NP-hard problem, was considered [?].

2. Estimation of s^* the projection of c onto admissible constraints. Find a trajectory by projection of the given input parametrized curve c onto a set of admissible curves S . The curve is said to be admissible if $s \in S \cap A$ where S is defined as

$$S := \{s \in (C^2([0, T]))^d, \|s\| \leq \alpha, \|\ddot{s}\| \leq \beta\} \quad (6)$$

where $\alpha = \gamma G_{max}$ and $\beta = \gamma S_{max}$ and A denotes the set of affine constraints,

$$A := \{s : [0, T] \rightarrow \mathbb{R}^d, A(s) = v\} \quad (7)$$

where v is a vector of parameters in \mathbb{R}^p (p is the number of additional constraints) and A essentially is a linear mapping from the curves space to projection space \mathbb{R}^p .

However, as a result of the discretization, the curve s is in $\mathbb{R}^{n.d}$ instead of \mathbb{R}^p where n is the number of time points and $s(i) \in \mathbb{R}^d$ denotes the curve location at time $(i-1)\delta t$ with $\delta t = \frac{T}{n-1}$. If the first-order differential operator be represented by a matrix $\dot{M} \in \mathbb{R}^{n.d \times n.d}$ i.e. $\dot{s} = \dot{M}s$ and the discrete second-order differential operator is defined as $\ddot{M} = -\dot{M} * \dot{M} \in \mathbb{R}^{n.d \times n.d}$. Then, S in the discrete domain can now be defined as $S := \{s \in \mathbb{R}^{n.d}, \|\dot{M}s\| \leq \alpha, \|\ddot{M}s\| \leq \beta\}$.

In essence, the primal problem that is considered in this domain is as follows :

$$s^* := \underset{s \in S \cap A}{\operatorname{argmin}} \frac{1}{2} \|s - c\|_2^2 \quad (8)$$

where $\|s - c\|_2^2 := \int_0^T \|s(t) - c(t)\|_2^2 dt$.

Some of the important differences between Chauffert's [?] and Lustig's [?] optimal control theory approach are: (i) The solutions s^* and c have different support; (ii) the sets composed of the discretization of c and s^* at a given sampling rate are close to each other; (iii) the acquisition time T is fixed and equal to that of input curve c . Note that the time taken to retrace a curve is generally different from time for optimal reparametrization.

Two importance inferences were drawn from the aforementioned work (i) Using a lower velocity (10% and 50 % of maximal speed, γG_{max} were investigated) during the initial parametrization, results in a sampling density that approximates target density better; preserving the maximum number of target density samples, especially those located close to center of k -space. In spite of superior performance, the trajectory derived from low velocity (10%) was not considered a practical solution due to long duration of traversal; (ii) Chauffert et al. considered only the case of moving at constant velocity during the entire scan.

On careful examination followed by experimentation, we realized that moving with constant velocity at all instants irrespective of the location of the sample, in k -space, goes against the intuition of VDS scheme where samples close to center of k -space are drawn with higher probability compared to those at larger distances. Hence, we propose an additional constraint on the projection algorithm during its initial parametrization of velocity based on the location or position of the sample belonging to the chosen target distribution (2-D or 3-D). In this paper, only 2-dimensional space has been considered though it can be easily be extended to three dimension space.

We propose the following modified algorithm for the initial maximal velocity based parametrization by Chauffert et al. [?]:

Input: Maximal Velocity, v_{max} ; Sampling interval, δt ; Coordinate locations of discretized trajectory obtained on solving TSP, $s(i)$); **Distance of furthest sample in the TSP-solved trajectory**, d_k , from the center of k -space.

Output: Parametrized curve derived from **Position-based Variable Speed**

Constraint

- (i) Compute the dynamic step size, d_{dstep} with $d_{max} = v_{max} * \delta t$

$$d_{dstep} = d_{max} * \min(p(s), 1). \quad (9)$$

where p , a function of parametrized curve s , is responsible for smoothing the curve dynamically with respect to the position of the curve, and is defined as

$$p(s) = \frac{\|s(i)\|_2}{d_k} + \kappa \quad (10)$$

where κ is a small constant used to choose the fine smoothing desired closer to the center of the k -space where $\|s(i)\|_2 \rightarrow 0$ and $p(s) \rightarrow \kappa$.

Note that this step is the modification to the algorithm, instead of $d_{step} = v_s * \delta t$, where d_{step} refers to the fixed step size based on constant velocity, v_s such that $v_s \leq v_{max}$ and $d_{step} \leq d_{max}$.

- (ii) Determine the direction vector between $s(i + 1)$ and $s(i)$ and their $L2$ norm distance.
- (iii) Using the direction vector, relative distance and error term (set to zero in the first step), compute the number the steps required to reach the next point in the determined direction, moving in the steps of size d_{max} .
- (iv) Compute the error between the point reached by taking the discrete steps and the true destination derived from the target density. Store it in memory for next iteration.
- (v) Repeat the steps (i) to (iv) passing through sets of all consecutive points

The modification in step (i) allows finer control over parametrization near the center of k -space as the step size dynamically changes with respect to the $L2$ norm distance of the projected point from origin on admissible curve.

In addition, the constraint was enforced such that it does not violate any of the practical limits set previously - the maximum gradient, maximum slew-rate

and the maximum traversal speed. The proposed modified method mimics multi-resolution technique and enables high resolution scanning on a low resolution device by giving importance to samples at the k -space center. Thus, it can be concluded that the modification results in a physically plausible k -space trajectory satisfying gradient and slew rate constraints.

To demonstrate the modified projection method, a simple trajectory obtained by solving TSP on 500 points drawn randomly from π distribution was considered as reference [?] and it was assumed that there is no error on the k -space sample locations. The parameters and constraints used while designing the trajectory are as follows:

Maximum gradient, $G_{max} = 40e - 3 \text{ T/m}$;

Maximum slew-rate, $S_{max} = 150e - 3 \text{ T/m/ms}$;

Maximum span of k -space, $K_{max} = 512 \text{ m}^{-1}$;

$\gamma = 42.576 \text{ MHz/T}$.

Sampling rate, $\Delta t = 4 \mu\text{s}$.

For comparison between the position-constrained projection method and chauffert et al. projection method, both 10% and 50% of maximum velocity were initially considered as they correspond to the velocity with which our method traces the trajectory at regions close to center of k -space for $\kappa = 0.1$ and 0.5 respectively. However, the time taken to trace the trajectory at 10% of v_{max} is too long (by a factor of five) and is not feasible in practice as stated in [?], hence, was neglected for further analysis. The Fig. 12 shows the TSP-solved (in blue) and smoothed trajectory (in red), along with slew rate and gradients plots (second and third coulmns), for Chauffert's method (at 50% Max. Velocity) and the proposed method for three levels of smoothness corresponding to $\kappa = 0.5$, 0.25 and 0.1 respectively.

The levels of smoothing can be inferred from the degree of closeness between the proposed (in red) and the raw TSP solved trajectory (in blue). It was observed in rows 2-4 of Fig. 12 that it decrease with increase in κ . The time-taken to scan by the aforementioned methods are 8.732, 10.424, 14.308, 20.308 ms respectively. The final k -space trajectories obtained from the proposed

method and its corresponding scan timings show the ability of the modified method to approximate the target density better with slight increase in scan time.

Next, we show the performance of modified projection method on the sampling pattern obtained from k -ABC algorithm using the magnitude k -space of In-vivo Brain image as the fitness distribution. The time taken to scan the samples was found to be 27.92 ms, 35.51 ms, 51.51 ms and 75.98 ms. In Fig. 13, we show the k -ABC based VDS sampling scheme (top-left), raw TSP solved trajectory (top-right), k -space trajectory based on Chauffert's method with maximal velocity (middle-left) and the proposed method for $\kappa = 0.5$ (middle-right), 0.25 (bottom-left) and 0.1 (bottom-right) respectively. By overlaying a discrete Cartesian k -space on the sampling trajectory, such that a sample is measured if the sampling trajectory crosses the corresponding cell of the k -space grid, the sampling pattern for each case was found. Using which reconstruction was performed to test the image quality metrics. It was observed that the sampling pattern obtained using modified projection algorithm, with $\kappa=0.1$, results in the best PSNR = 26.6326 dB, SSIM = 0.552 and HFEN = 2.0419 as compared to the PSNR = 16.6756 dB, SSIM = 0.3888 and HFEN = 4.138 obtained from unmodified projection method.

However, keeping in the mind the trade-off between time taken to scan and the quality of reconstructed image, we propose the use of the sampling trajectory obtained by setting $\kappa=0.25$ as it results in a 6 dB improvement in PSNR = 22.77 dB over the projection method, and SSIM = 0.5901 and HFEN = 2.467 with just 4 ms increase in scan time.

The main contribution of the proposed position-constrained projection method is in designing a k -space trajectory that is physically plausible yet, preserves characteristics of a VDS scheme which is adapted to k -space of region of interest, prior to the scan.

4. Conclusion

In this paper, we have proposed a novel approach to design an adaptive variable density sampling scheme utilising the unique foraging abilities of the bee colony. A modified artificial bee colony algorithm (k -ABC algorithm) has been developed using only few design parameters which utilizes the concept of sampling in circular bins to generate an adaptive VDS sampling scheme, for both single slice and multi-slice imaging, based on principles of CS. Different aspects of the k -ABC algorithm - i) effect of varying food source distribution, ii) insight into parameter selection, iii) image quality for different under-sampling percentages, iv) k -ABC adaptive VDS scheme performance with different distributions, v) robustness of the k -ABC algorithm, vi) k -ABC adaptive VDS scheme performance at different under-sampling percentages, vii) sampling scheme for Multi-slice/ROI volume imaging and viii) practical implementation of scan trajectory, were illustrated through examples and extensive simulations. It was first shown that the sampling pattern generated with low under-sampling percentage of 5% and 10% by k -ABC adaptive algorithm gives significant improvement in reconstruction of images. Then, a modified projection algorithm was proposed which allows finer control over parametrization near the center of k -space as the step size dynamically changes with respect to the L_2 -distance of the projected point, from origin on the admissible curve, instead of the fixed step size based on constant velocity. Finally, using the modified projection method, it was demonstrated that the proposed method results in a physically plausible k -space trajectory adapted to a reference k -space improves the image quality of reconstructed image by a significant value with just a slight increase in scan time.

References

- [1] E. J. Candès, J. Romberg, T. Tao, Robust uncertainty principles: Exact signal reconstruction from highly incomplete frequency information, Information Theory, IEEE Transactions on 52 (2) (2006) 489–509.

- [2] M. Lustig, D. Donoho, J. M. Pauly, Sparse mri: The application of compressed sensing for rapid mr imaging, *Magnetic resonance in medicine* 58 (6) (2007) 1182–1195.
- [3] H. Wang, D. Liang, L. Ying, Pseudo 2d random sampling for compressed sensing mri, in: 2009 Annual International Conference of the IEEE Engineering in Medicine and Biology Society, IEEE, 2009, pp. 2672–2675.
- [4] C. Boyer, P. Weiss, J. Bigot, An algorithm for variable density sampling with block-constrained acquisition, *SIAM Journal on Imaging Sciences* 7 (2) (2014) 1080–1107.
- [5] F. Knoll, C. Clason, C. Diwoky, R. Stollberger, Adapted random sampling patterns for accelerated mri, *Magnetic resonance materials in physics, biology and medicine* 24 (1) (2011) 43–50.
- [6] B. Adcock, A. C. Hansen, C. Poon, B. Roman, Breaking the coherence barrier: A new theory for compressed sensing, arXiv preprint arXiv:1302.0561.
- [7] S. Ravishankar, Y. Bresler, Adaptive sampling design for compressed sensing mri, in: Engineering in Medicine and Biology Society, EMBC, 2011 Annual International Conference of the IEEE, 2011, pp. 3751–3755. doi:10.1109/IEMBS.2011.6090639.
- [8] N. Chauffert, P. Ciuciu, J. Kahn, P. Weiss, Variable density sampling with continuous sampling trajectories, *SIAM Journal on Imaging Sciences*.
- [9] J. Vellagoundar, R. R. Machireddy, An improved variable density sampling for compressive sampling mri, *Journal of Medical Imaging and Health Informatics* 5 (4) (2015) 730–736.
- [10] C. Krishna, K. Rajgopal, Adaptive variable density sampling based on knapsack problem for fast mri, in: 2015 IEEE International Symposium on Signal Processing and Information Technology (ISSPIT), IEEE, 2015, pp. 364–369.

- [11] D. Karaboga, B. Gorkemli, A combinatorial artificial bee colony algorithm for traveling salesman problem, in: Innovations in Intelligent Systems and Applications (INISTA), 2011 International Symposium on, 2011, pp. 50–53.
doi:10.1109/INISTA.2011.5946125.
- [12] A. Rekaby, A. Youssif, A. Sharaf Eldin, Introducing adaptive artificial bee colony algorithm and using it in solving traveling salesman problem, in: Science and Information Conference (SAI), 2013, 2013, pp. 502–506.
- [13] H. Rauhut, Compressive sensing and structured random matrices, Theoretical foundations and numerical methods for sparse recovery 9 (2010) 1–92.
- [14] American radiology services.
URL <http://www3.americanradiology.com/pls/web1/wwmain.home>
- [15] S. Ravishankar, Y. Bresler, Mr image reconstruction from highly undersampled k-space data by dictionary learning, Medical Imaging, IEEE Transactions on 30 (5) (2011) 1028–1041.
- [16] Z. Wang, A. C. Bovik, H. R. Sheikh, E. P. Simoncelli, Image quality assessment: from error visibility to structural similarity, Image Processing, IEEE Transactions on 13 (4) (2004) 600–612.
- [17] M. Aharon, M. Elad, A. Bruckstein, K-svd: An algorithm for designing overcomplete dictionaries for sparse representation, Signal Processing, IEEE Transactions on 54 (11) (2006) 4311–4322.
- [18] Y. C. Pati, R. Rezaifar, P. Krishnapra

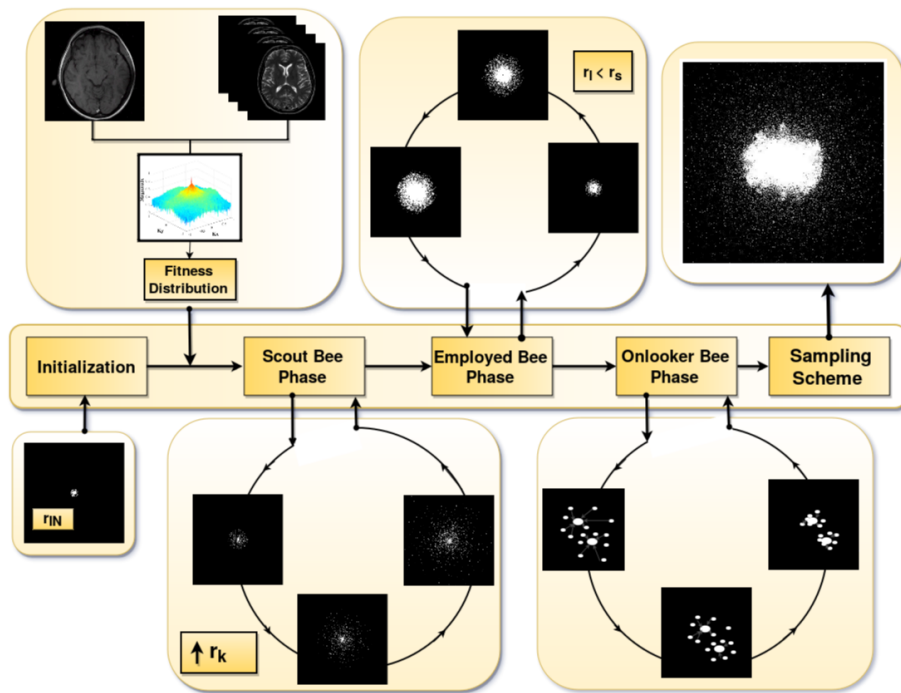


Figure 1: Flow Chart of k -ABC Algorithm

Algorithm: *k*-ABC

Input : Initial Food sources N_0 , Initial search radius r_{IN} , Swarm size of the employed-bees M , Bin Width Δr , Maximal radius for neighbourhood search r_s and Fitness distribution $f(x)$.

Output: Variable Density Sampling scheme

- 1 Initialize the bee population with N_0 - food sources
 - 2 Pick N_k food sources randomly from each bin using (2).
 - 3 Pass the M best nectar locations within r_s of k -space to the employed-bees and evaluate them.
 - 4 The employed-bees perform a neighbourhood search to find better nectars locally according to (3). evaluate and select them based on the constraint in (4) which results in N_k^e samples/bin.
 - 5 The onlooker-bees choose the E best nectars, from the available N_k^e nectars, based on a distance criterion and settle in their vicinity.
 - 6 Memorize the locations of all food sources selected by scout, employed and onlooker-bees in the bin, N_k^o .
 - 7 Repeat the steps **2-6** for all bins.
 - 8 The final sampling pattern is obtained by logical OR of N_k^o over k bins.
-

Table 1: Image Quality Measure Comparison of Brain Image for Food Source Distribution as a function distance

| Food Source Distribution | Quality Measure | Undersampling (R) in % | | | |
|--------------------------|-----------------|----------------------------|---------------|---------------|---------------|
| | | 5 | 10 | 15 | 20 |
| Exponentially Decreasing | PSNR | 31.59 | 35.88 | 38.93 | 41.21 |
| | SSIM | 0.8848 | 0.9458 | 0.9660 | 0.9799 |
| Uniform distribution | PSNR | 30.80 | 35.04 | 37.85 | 40.67 |
| | SSIM | 0.8728 | 0.9256 | 0.9556 | 0.9756 |
| Exponentially Increasing | PSNR | 25.62 | 33.06 | 35.53 | 36.56 |
| | SSIM | 0.7205 | 0.9152 | 0.9406 | 0.9766 |

Table 2: Image Quality of Reconstruction Results for Brain Image for different under-sampling percentages ($R\%$)

| Parameters | | | | $R\%$ | Quality Measures | | | | | | | | |
|------------|-------|-----|----|--------------|------------------|----------|-------------|-------|----------|-------------|-------|----------|--|
| N_0 | r_s | M | | PSNR | μ | σ | HFEN | μ | σ | SSIM | μ | σ | |
| 1300 | 0.67 | 75 | 20 | 43.71 | 43.66 | 0.009 | 0.30 | 0.28 | 0.001 | 0.97 | 0.966 | 1.93e-06 | |
| 1400 | 0.60 | 45 | 15 | 42.39 | 42.48 | 0.004 | 0.52 | 0.49 | 0.007 | 0.95 | 0.95 | 1.01e-05 | |
| 1200 | 0.50 | 35 | 10 | 40.86 | 40.85 | 0.013 | 0.80 | 0.80 | 0.002 | 0.94 | 0.93 | 7.57e-05 | |
| 900 | 0.40 | 10 | 5 | 36.92 | 36.28 | 0.4782 | 1.88 | 2.04 | 0.060 | 0.90 | 0.89 | 0.004 | |

Table 3: Reconstruction Quality of Brain Image for different VDS schemes for under-sampling (R) of 10% and 5%

| VDS Scheme | PSNR | | HFEN | | SSIM | |
|---------------------------------------|--------------|--------------|-------------|-------------|-------------|-------------|
| | 10% | 5% | 10% | 5% | 10% | 5% |
| k -ABC (Gaussian distribution) | 40.86 | 36.92 | 0.80 | 1.88 | 0.94 | 0.90 |
| k -ABC (π -distribution) | 40.51 | 36.41 | 0.91 | 2.02 | 0.93 | 0.89 |
| k -ABC (In-Vivo Brain distribution) | 41.03 | 36.79 | 0.73 | 1.90 | 0.95 | 0.91 |
| k -ABC (T2 Sag Spine distribution) | 40.78 | 36.53 | 0.88 | 1.99 | 0.94 | 0.91 |
| Adaptive Sampling Scheme[?] | 39.79 | 34.83 | 0.94 | 1.63 | 0.89 | 0.80 |
| Independent π -distribution[?] | 37.31 | 33.68 | 1.82 | 3.06 | 0.90 | 0.89 |

Table 4: Reconstruction Quality of Spinal Image for different VDS schemes for under-sampling (R) of 10% and 5%

| VDS Scheme | PSNR | | HFEN | | SSIM | |
|---------------------------------------|--------------|--------------|-------------|-------------|-------------|-------------|
| | 10% | 5% | 10% | 5% | 10% | 5% |
| k -ABC (Gaussian distribution) | 36.27 | 31.59 | 1.67 | 3.49 | 0.94 | 0.89 |
| k -ABC (π -distribution) | 35.56 | 31.14 | 1.81 | 3.75 | 0.94 | 0.88 |
| k -ABC (In-vivo Brain distribution) | 35.43 | 31.67 | 1.87 | 3.44 | 0.94 | 0.89 |
| k -ABC (T2 Sag Spine distribution) | 36.57 | 31.68 | 1.51 | 3.47 | 0.95 | 0.89 |
| Adaptive Sampling Scheme[?] | 34.58 | 27.91 | 1.70 | 3.14 | 0.91 | 0.78 |
| Independent π -distribution[?] | 32.33 | 29.19 | 3.30 | 4.98 | 0.89 | 0.84 |

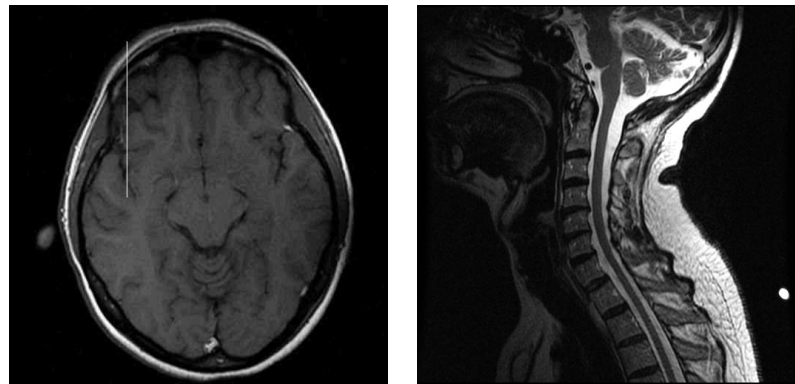


Figure 2: **Reference Images:** In-Vivo MRI Brain Image (left) and T2 Sagittal Spine Image (right)

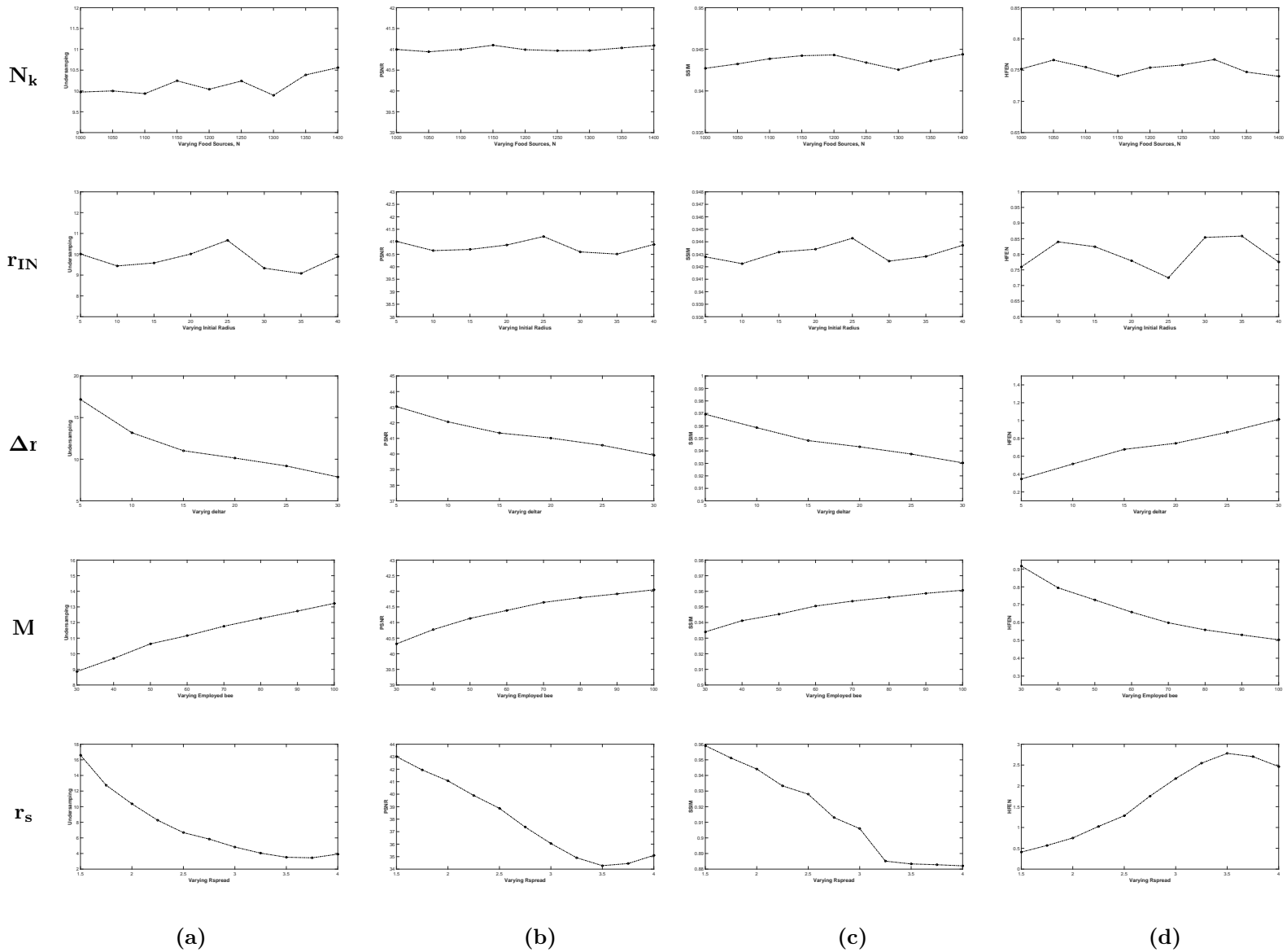


Figure 3: Range of Variation of Image Quality of Metrics: (a) Undersampling, (b) PNSR, (c) HFEN and (d) SSIM with respective parameters of K-ABC Algorithm mentioned in *Left-most Coloumn*

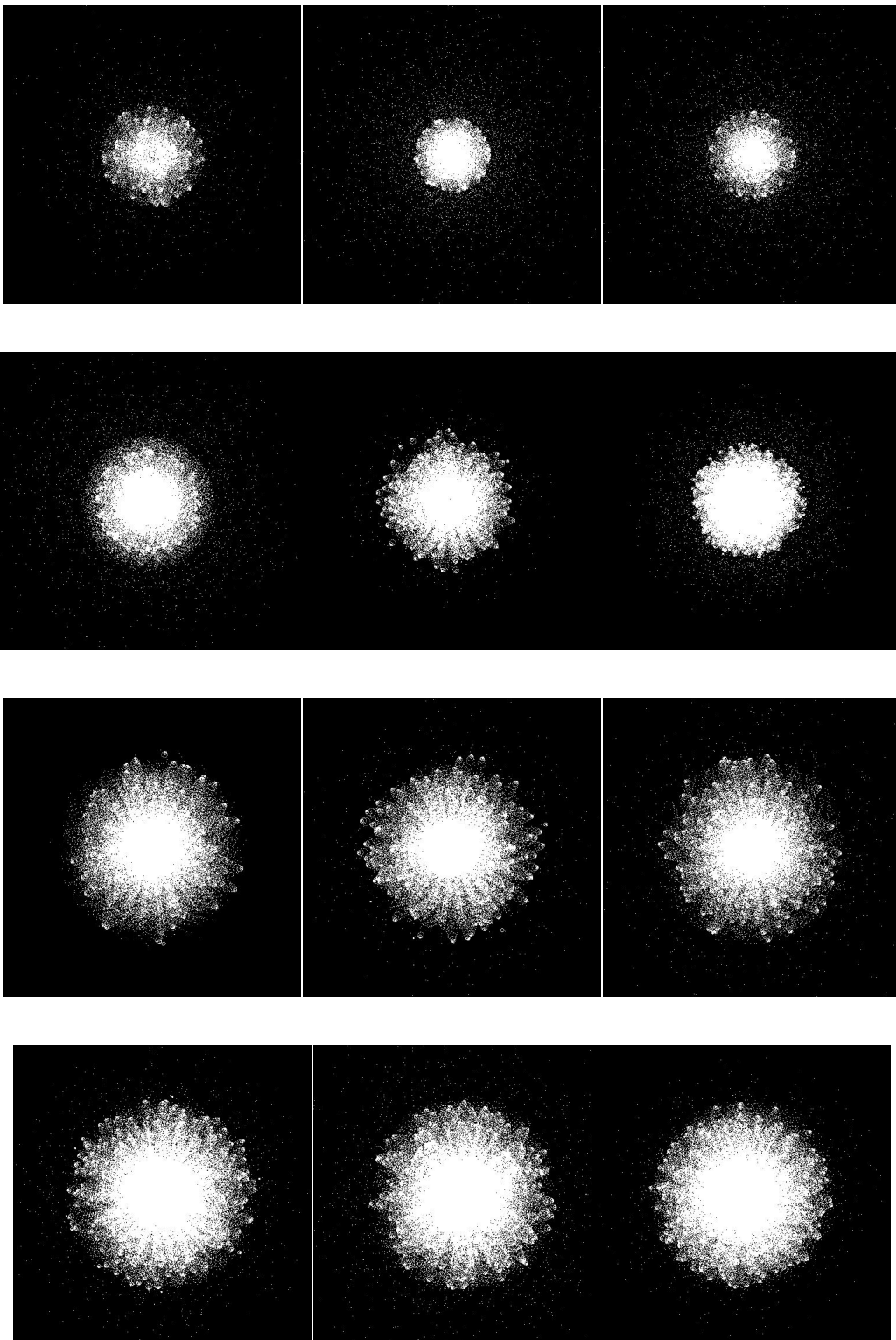


Figure 4: **Monte Carlo Based Sampling Schemes:** with *Rows 1-4* referring to undersampling percentages 5, 10, 15 and 20 % respectively

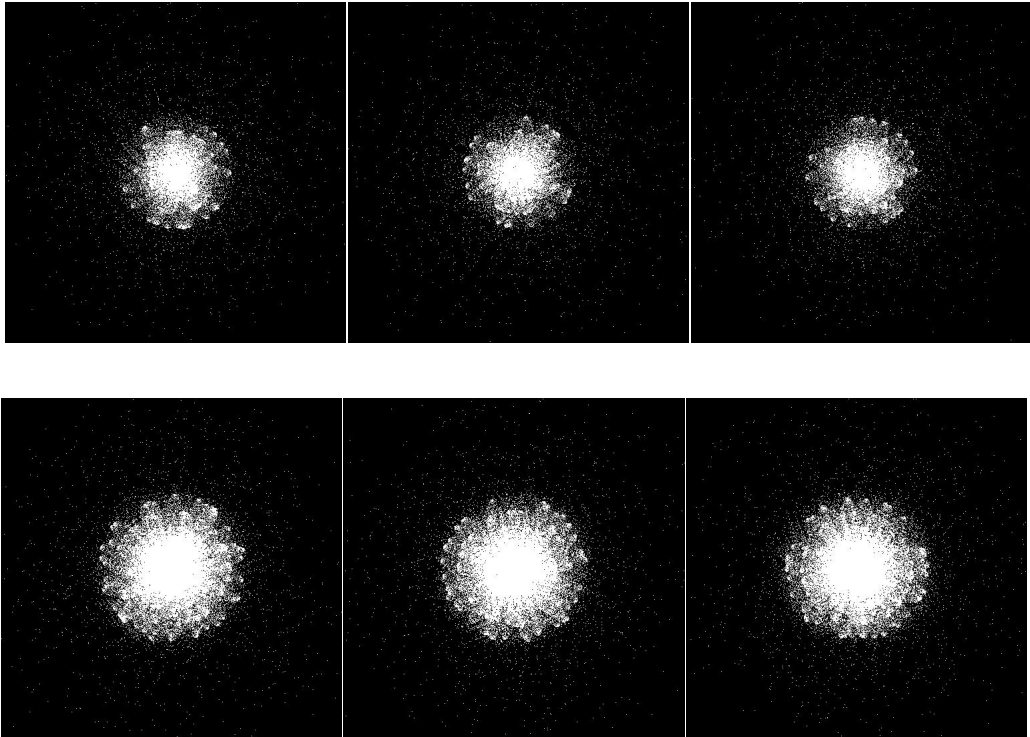


Figure 5: **Visualization of Sampling Schemes:** To test Robustness of the k -ABC algorithm for 5% (*Top-Row*) and 10% (*Bottom Row*)

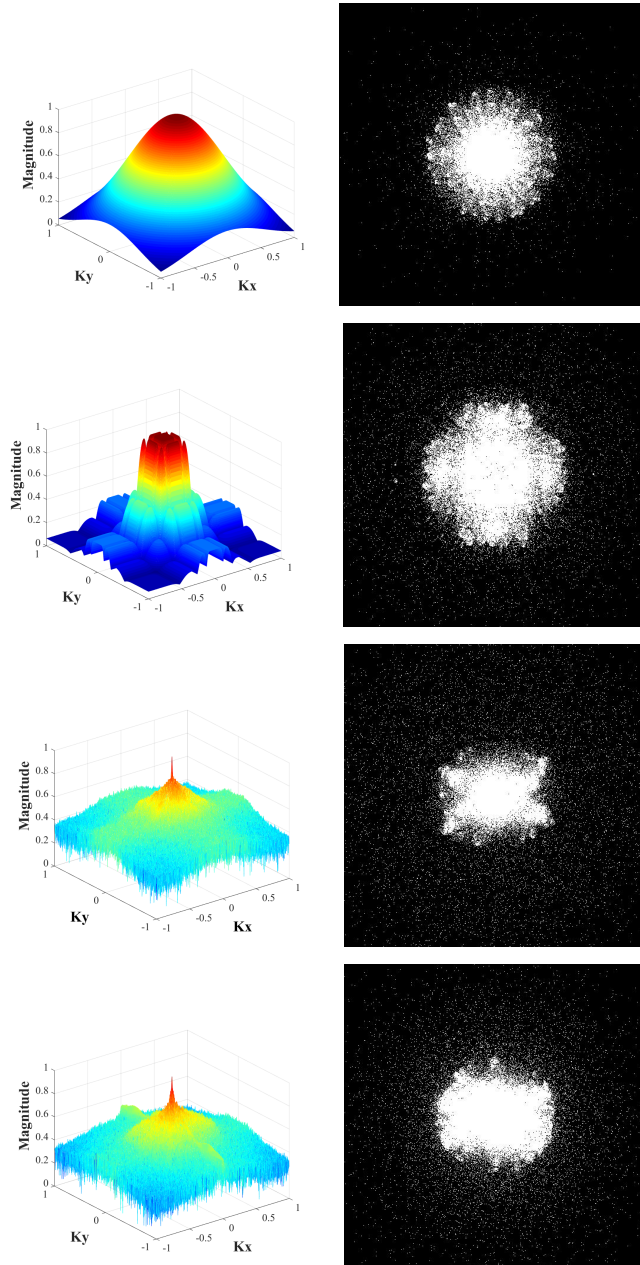


Figure 6: **Fitness-Value Distribution and the Corresponding VDS Patterns:** *Left Column* : Fitness Functions- Gaussian, and π -distribution, Magnitude k -space of brain image and sagittal spine image *Right Column* : Sampling Patterns for $R=10\%$ corresponding to the distributions.

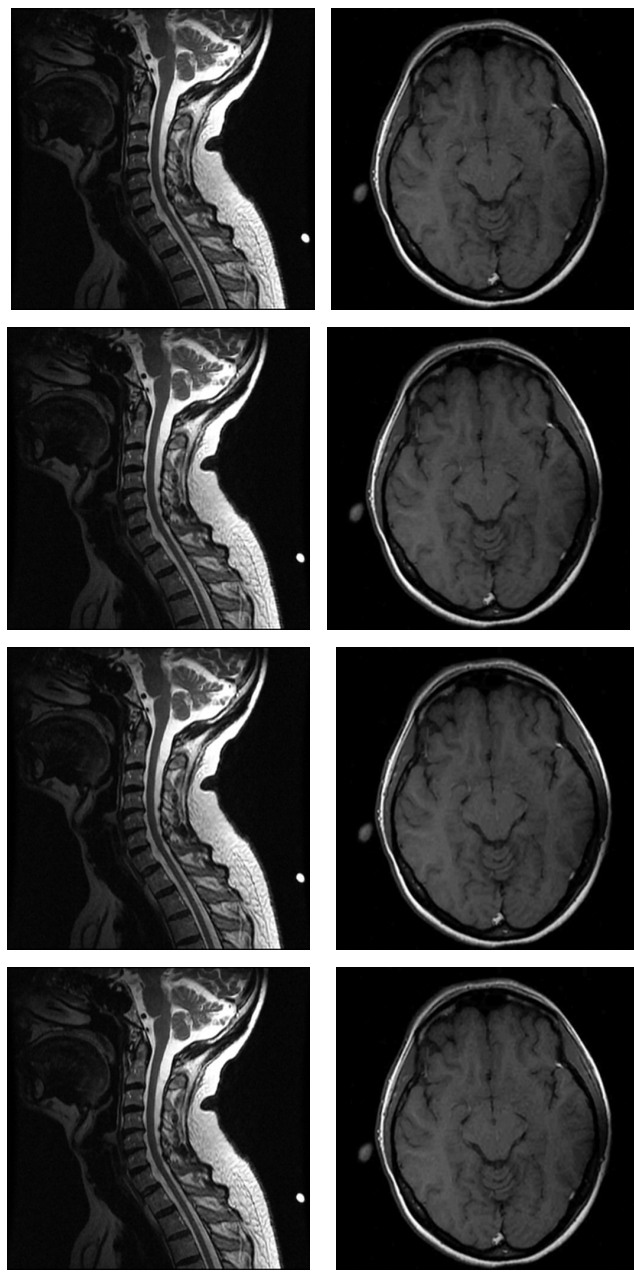


Figure 7: Reconstructed Images for varying Fitness Distribution: With Reconstructed T2-Weighted Sagittal Spinal (*left-coloumn*) and Brain Image (*right-coloumn*) for sampling schemes (as mentioned in Table 3 and 4) generated using Gaussian (*Row 1*), π -distribution (*Row-2*), Magnitude k -space of In-vivo brain (*Row-3*) image and sagittal spine image *Row-4* as fitness distribution.

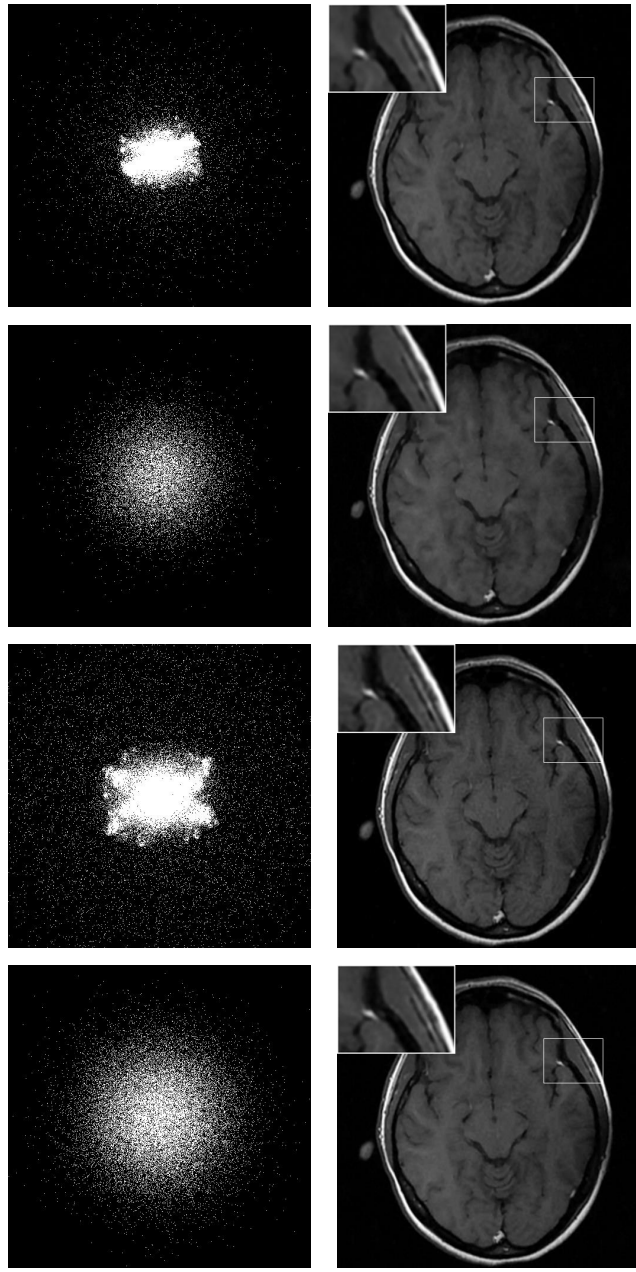


Figure 8: **Adaptive Sampling Pattern and Reconstructed Brain Image With k -ABC and Saiprasad et al. based sampling scheme shown alternatively for $R=5\%$ (Rows 1-2) and 10% (Rows 3-4).** The inset shows the magnified image of the rectangle area.

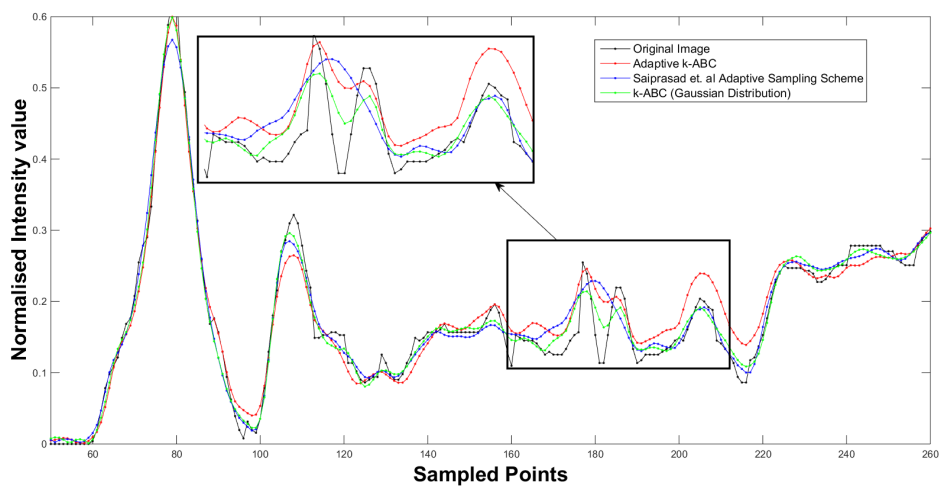


Figure 9: **Intensity profile comparison:** Along the line $X=160$ and $Y=[50:260]$ of In vivo Brain image as shown in Fig. 2

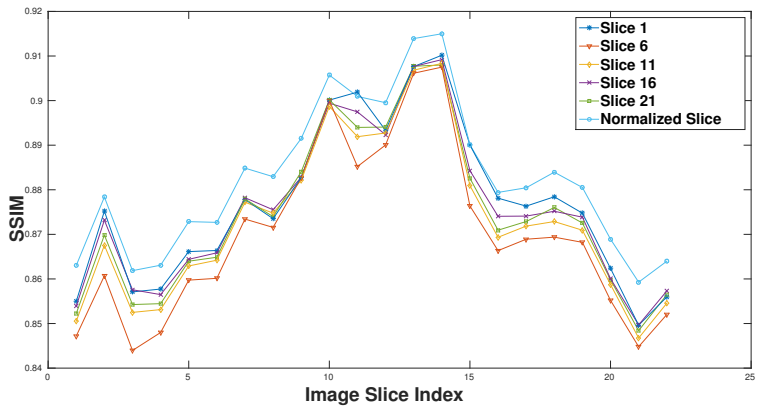
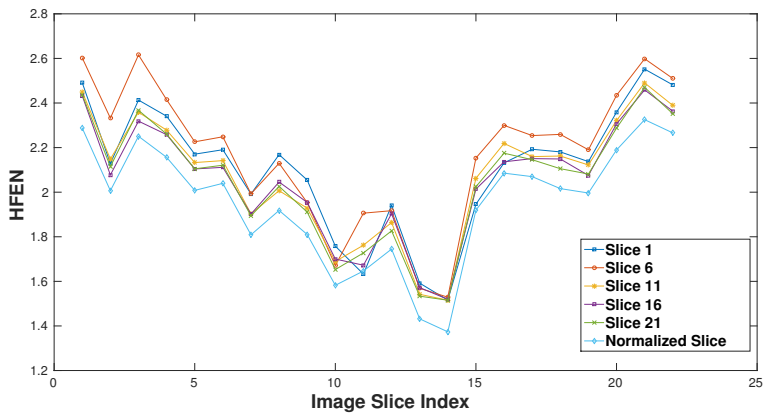
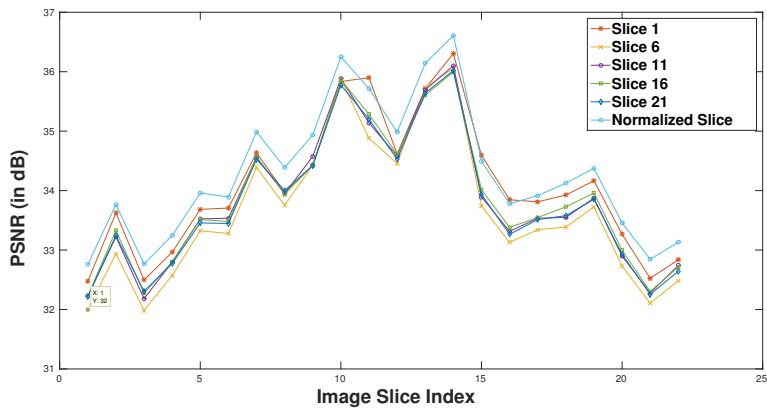


Figure 10: **Image Quality Metrics for the Knee Volume** With PSNR, HFEN and SSIM shown in rows *top*, *middle* and *bottom* respectively

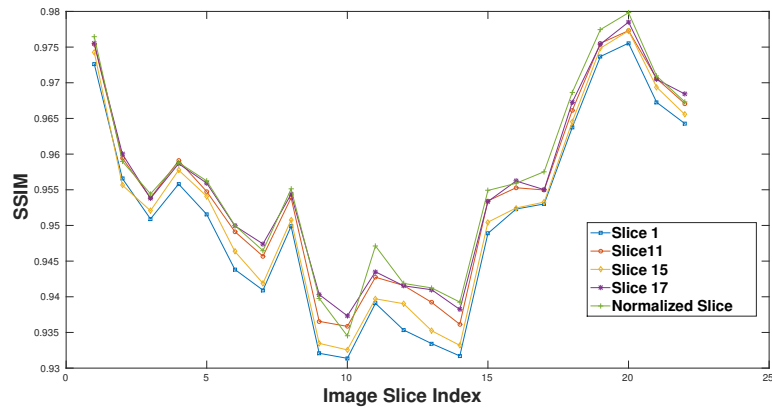
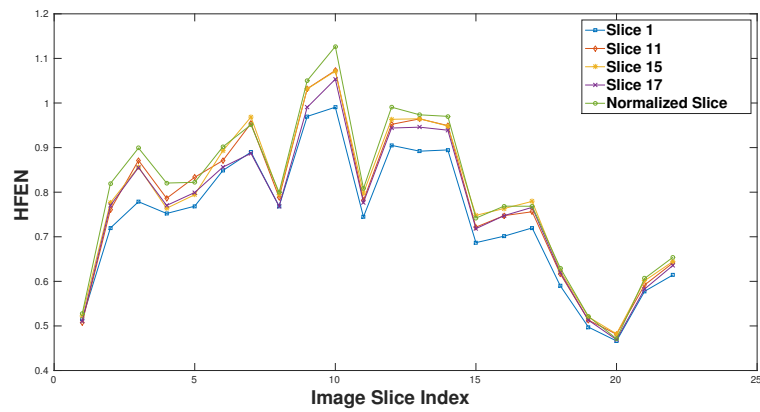
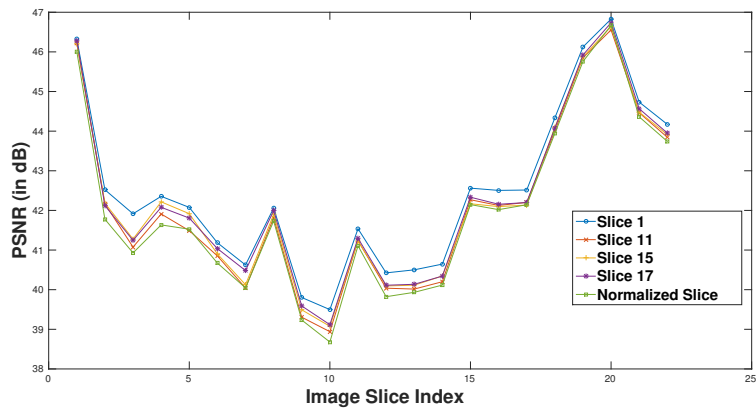


Figure 11: **Image Quality Metrics for the Brain Volume** With PSNR, HFEN and SSIM shown in rows *top*, *middle* and *bottom* respectively

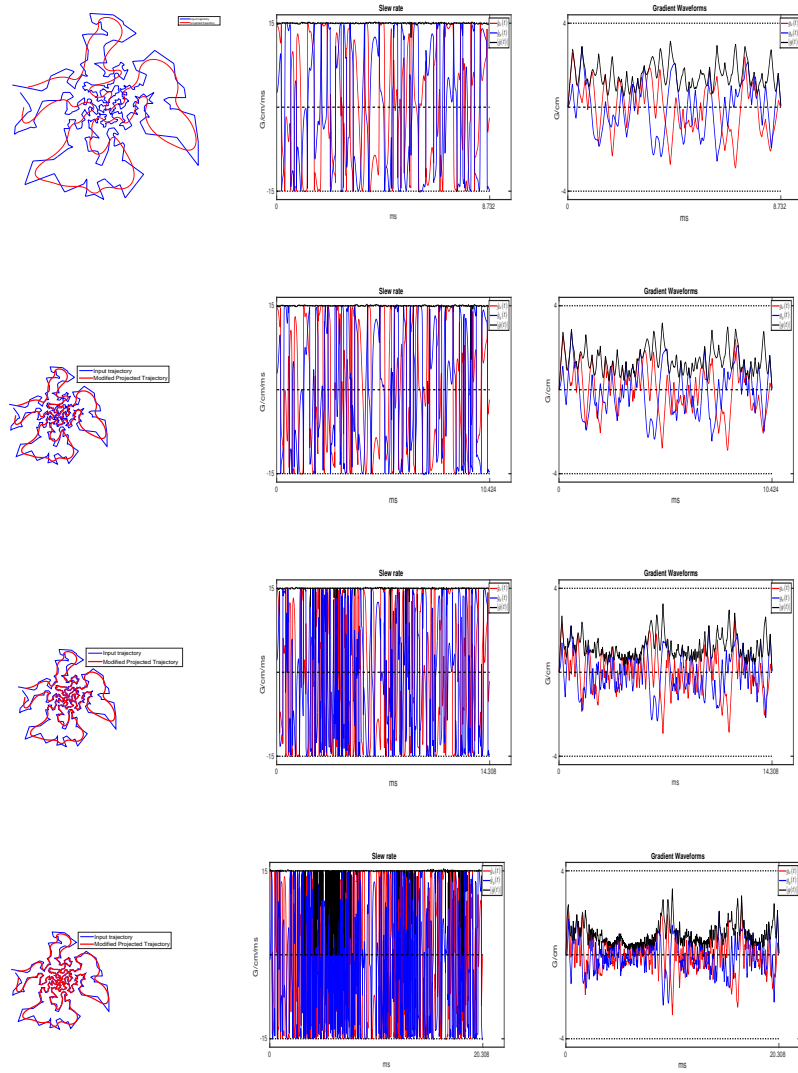


Figure 12: **TSP Solved Trajectory with Gradient and Slew Rate Plots:** With Chauffert et al. Projection method for 50% of Maximum Velocity shown in *Row-1* and proposed method for $\kappa=0.5, 0.25$ and 0.1 shown in *Rows 2, 3* and *4* respectively

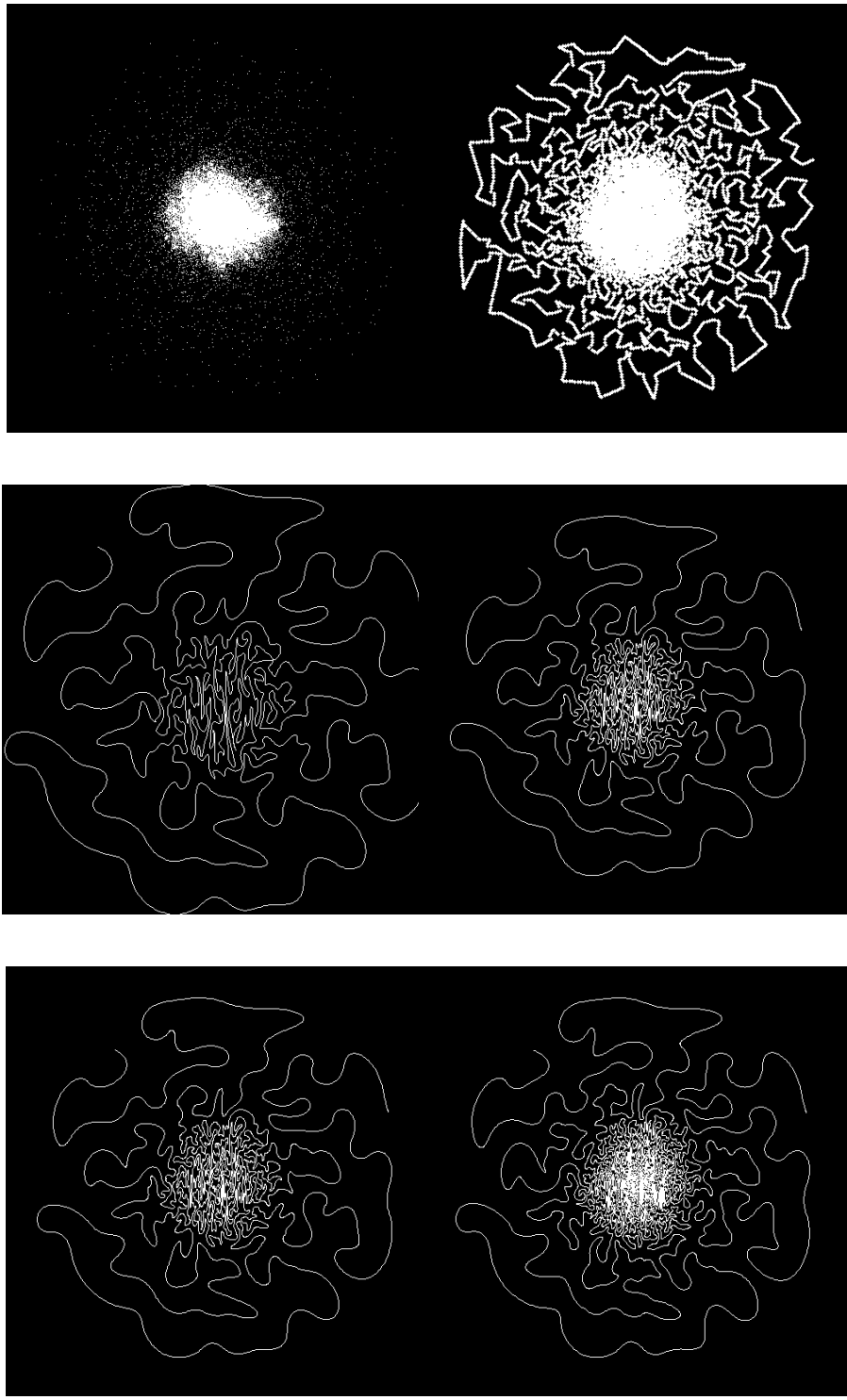


Figure 13: Trajectory Design for Adaptive K-ABC Sampling scheme for $R = 5\%$
With *Top-Row*: showing Adaptive K-ABC Sampling scheme for $R = 5\%$ (Left) and TSP-Solved Trajectory for the same (Right); *Middle-Row*: showing Chauffert's Projection Method for 50% of Maximum Velocity (Left) and Proposed Method for $\kappa = 0.5$ (Right); *Bottom-Row* Proposed Method for $\kappa=0.25$ (Left) and 0.1 (Right).